Author/s:
Li, C;Gu, X;Chen, Z;Han, X;Yu, N;Wei, Y;Gao, J;Chen, H;Zhang, M;Wang, A;Zhang, J;Wei, Z;Peng, Q;Tang, Z;Hao, X;Zhang, X;Huang, H

Title:
Achieving Record-Efficiency Organic Solar Cells upon Tuning the Conformation of Solid Additives

Date:
2022-08-17

Citation:
Li, C., Gu, X., Chen, Z., Han, X., Yu, N., Wei, Y., Gao, J., Chen, H., Zhang, M., Wang, A., Zhang, J., Wei, Z., Peng, Q., Tang, Z., Hao, X., Zhang, X. & Huang, H. (2022). Achieving Record-Efficiency Organic Solar Cells upon Tuning the Conformation of Solid Additives. Journal of the American Chemical Society, 144 (32), pp.14731-14739. https://doi.org/10.1021/jacs.2c05303.

Persistent Link:
https://hdl.handle.net/11343/334502

JACS
JOURNAL OF THE AMERICAN CHEMICAL SOCIETY
pubs.acs.org/JACS
Article

Achieving Record-Efficiency Organic Solar Cells upon Tuning the Conformation of Solid Additives

Congqi Li, Xiaobin Gu, Zhihao Chen, Xiao Han, Na Yu, Yanan Wei, Jinhua Gao, Hao Chen, Meng Zhang, Ao Wang, Jianqi Zhang, Zhixiang Wei, Qian Peng, Zheng Tang, Xiaotao Hao, Xin Zhang,* and Hui Huang*

Cite This: J. Am. Chem. Soc. 2022, 144, 14731−14739
Read Online
ACCESS | Metrics & More | Article Recommendations | Supporting Information

ABSTRACT: Volatile solid additives (SADs) are considered as a simple yet effective approach to tune the film morphology for high-performance organic solar cells (OSCs). However, the structural effects of the SADs on the photovoltaic performance are still elusive. Herein, two volatilizable SADs were designed and synthesized. One is SAD1 with twisted conformation, while the other one is planar SAD2 with the S···O noncovalent intramolecular interactions (NIIs). The theoretical and experimental results revealed that the planar SAD2 with smaller space occupation can more easily insert between the Y6 molecules, which is beneficial to form a tighter intermolecular packing mode of Y6 after thermal treatment. As a result, the SAD2-treated OSCs exhibited less recombination loss, more balanced charge mobility, higher hole transfer rate, and more favorable morphology, resulting in a record power conversion efficiency (PCE) of 18.85% (certified PCE: 18.7%) for single-junction binary OSCs. The universality of this study shed light on understanding the conformation effects of SADs on photovoltaic performances of OSCs.

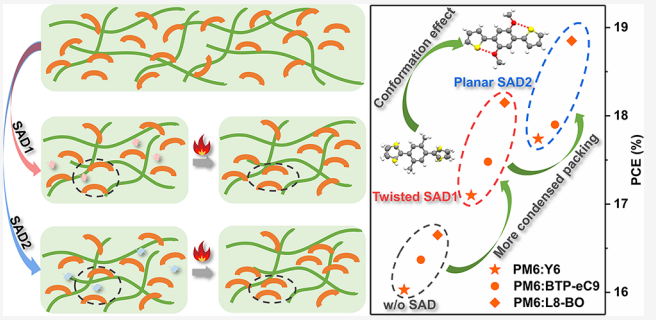

INTRODUCTION

In the past few years, the power conversion efficiencies (PCEs) of organic solar cells (OSCs) have stepped over 18%,[1−3] mainly due to the innovation in active layer materials and the engineering of charge-transfer interfaces.[4−10] In addition, another important focus is tuning the morphology of the bulk-heterojunction (BHJ) blend films, involving molecular orientation, crystallinity, and domain size and purity, which can greatly affect exciton diffusion and dissociation, charge transport, and recombination.[11−15] Therefore, several important strategies have been used to tune phase separation and film morphology, such as the solvent additive,[16−18] thermal annealing (TA),[19] and solvent vapor annealing,[20] resulting in the enhancement of photovoltaic performances.

Recently, volatile solid additives (SADs) have emerged as excellent candidates for optimizing the film morphology and photovoltaic performances.[21−30] In general, SADs can be divided into three types according to their working mechanisms. The first type of SADs can induce ordered and condensed intermolecular packing to form favorable morphology through the strong charge−quadrupole interaction or σ−hole interaction, thus leading to enhanced photovoltaic performance.[24−26] The second type of SADs can effectively decrease the adsorption energy of acceptors to improve π−π stacking through the attractive interaction between the SADs and acceptors, thereby resulting in an enhancement of light absorption and electron mobility.[27,28] The last type of SADs with high crystallinity can form well-developed nanoscale phase separation by restricting the over self-aggregation of acceptors in the process of film formation and then facilitating the donors to access the remaining space of SADs during the TA process.[29,30] Although these new strategies of SADs have shown many attractive features, the fundamental understanding of the relationship of SAD structures, active layer morphology, and OSC performance is missing.

Conformation is a basic parameter of organic compounds, which significantly influences their physicochemical properties. Usually, the planar conformation is critical to achieve high charge transport mobilities of organic/polymeric semiconductors. Thus, many efforts including covalent and noncovalent methods have been made to tune the conformation to achieve high performance organic/polymeric semiconductors for optoelectronics, such as OSCs,[31−34] thin-film transistors (OTFTs),[35−37] room temperature phosphorescence,[38,39] photodetectors (OPDs),[40] and so on. Among them, non-

Received: May 18, 2022
Published: July 20, 2022

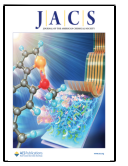

https://doi.org/10.1021/jacs.2c05303
J. Am. Chem. Soc. 2022, 144, 14731−14739

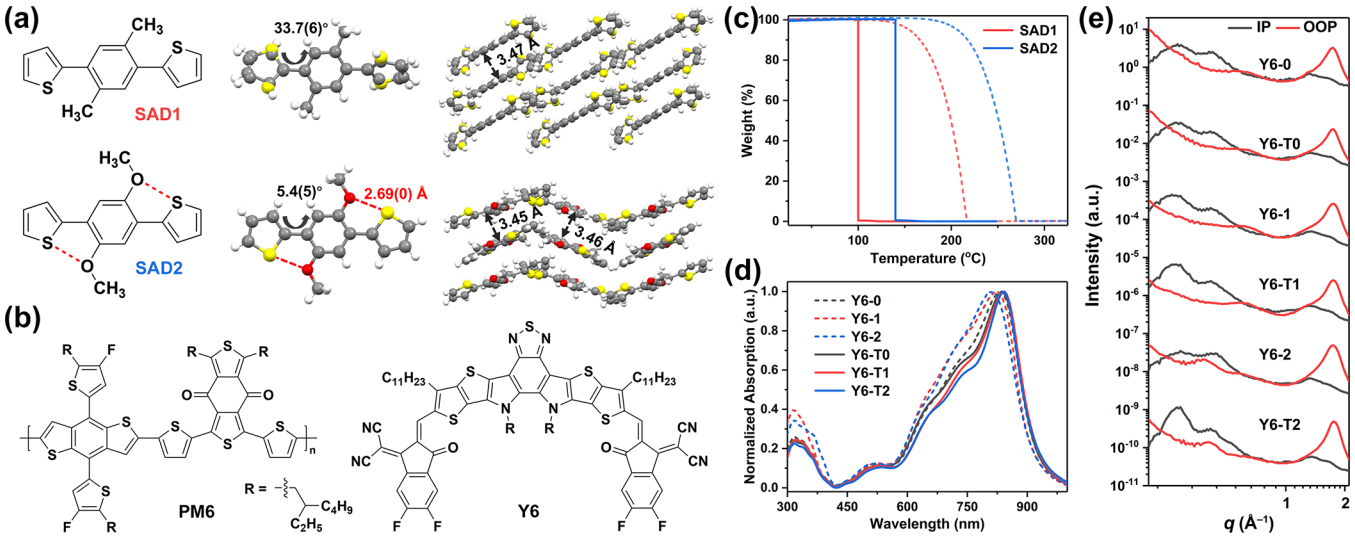

Figure 1. (a) Chemical structures, single-crystal structures, and molecular packing of SAD1 and SAD2. (b) Chemical structures of PM6 and Y6. (c) TGA plots of SAD1 and SAD2 at a scan rate of 5 °C min^{-1} (dash line). During the heating process, the temperature was held constant for 6 h at 100 °C for SAD1 and 140 °C for SAD2 (solid line). (d) UV−vis absorption spectra of Y6-0, Y6-1, and Y6-2 (dash line) and Y6-T0, Y6-T1, and Y6-T2 (solid line) films. (e) In-plane and out-of-plane cuts of the corresponding GIWAXS patterns.

covalent intramolecular interactions (NIIs) has been used as an important strategy to enhance the molecular rigidity and planarity[41−43] and thus the charge transport mobilities of the organic/polymeric semiconductors, since it can efficiently reduce the reorganization energy and suppress nonradiative decay.[44]

Herein, two SADs, a twisted-type SAD (SAD1) and a planar-type one (SAD2) with S···O NIIs (Figure 1a), were designed and synthesized to investigate the influence of the conformation of SADs on the photovoltaic performance of OSCs. The existence of S···O NIIs in SAD2 was supported by the single crystal X-ray structures and the optical spectroscopy, while the excellent volatility of both SADs was proven by the thermogravimetry analysis (TGA) and UV−vis absorption. The theoretical and experimental studies revealed that the planar SAD2 is beneficial to form a tighter $\pi-\pi$ stacking of Y6 (see Figure 1b) film than the twisted SAD1 after the addition/removal process. Thus, a mechanism was proposed that SAD2 with small space occupation can easily insert between Y6 molecules, which induced a tighter intermolecular packing mode of Y6 after the TA process, beneficial to the charge transport mobilities. As a result, SAD2-treated PM6:Y6-based OSCs exhibited a notable PCE of 17.74%, much higher than that of SAD1-treated ones (17.16%). The universal applications of these SADs in boosting photovoltaic performances were exemplified by the superior performance of the SAD2-treated PM6:L8-BO devices, which delivered an outstanding PCE of 18.85% (a certified value of 18.7%), the record for single-junction binary OSCs.

RESULTS AND DISCUSSION

Synthesis and Characterization of SADs. The synthetic route toward SAD1 and SAD2 is shown in Scheme S1. The Suzuki cross-coupling reaction between thiophen-2-ylboronic acid and 1,4-dibromo-2,5-dimethylbenzene (or 1,4-dibromo-2,5-dimethoxybenzene) afforded the two SADs, which were fully characterized by ^{1}H and ^{13}C NMR. To understand the role of NIIs on the molecular conformation, single-crystals of SADs were raised for X-ray diffraction (Table S1). The results showed that SAD1 (Figure 1a) bears a twisted geometry with a dihedral angle (θ) of 33.7(6)°, while SAD2 possesses an essentially planar backbone (θ = 5.4(5)°) with shorter S···O distances (d = 2.69(0) Å) than the sum of the van der Waals radius ($r_{w,\ S\cdots O}$ = 3.25 Å), verifying the existence of S···O NIIs.[45,46] Furthermore, SAD1 and SAD2 exhibited similar $\pi-\pi$ stacking distances [3.47(2) Å for SAD1 and 3.45(1) and 3.46(2) Å for SAD2] but different packing patterns. As demonstrated in Figure S1, the electrostatic potential (ESP) concentration in the conjugated backbone of SAD2 is relatively more negative than that of SAD1, which was ascribed to the electron-donating of oxygen atoms and the planar conformation of SAD2.[27] In addition, PM6 and Y6 exhibit identical and opposite ESP distributions with the two SADs, respectively, revealing that strong intermolecular interactions can be formed between Y6 and the SADs.[25]

The absorption and emission spectra of SADs in dilute chloroform solutions are shown in Figure S2a, and the corresponding data are summarized in Table S2. The absorption spectrum of the twisted SAD1 exhibited a maximum absorption peak (λ_{max}) at 294 nm, while SAD2 showed a more pronounced red-shift (λ_{max} = 358 nm) due to its more planar conformation. In addition, the emission peaks of SAD1 and SAD2 appeared at 368 and 397 nm, respectively. Thus, the Stokes shift ($\Delta\nu$) of SAD2 (2744 cm^{-1}) was found to be much smaller than that of SAD1 (6840 cm^{-1}), supporting that SAD2 possesses a more rigid backbone. In addition, absorption and emission spectra in film exhibited similar but redshifted spectral shapes compared with those in solution (Figure S2b). As expected, a smaller Stokes shift value was observed for SAD2 (3879 cm^{-1}) in film in comparison with that for SAD1 (6440 cm^{-1}). Furthermore, the reorganization energies in the $S_0 \rightarrow S_1$ transition were calculated to be 9.66 and 4.26 kcal mol^{-1} for SAD1 and SAD2, respectively, suggesting that the introduction of S···O NIIs can effectively limit the geometric relaxation. These above findings proved that SAD2 possessed an enhanced molecular planarity and rigidity due to the existence of S···O NIIs.

https://doi.org/10.1021/jacs.2c05303
J. Am. Chem. Soc. 2022, 144, 14731−14739

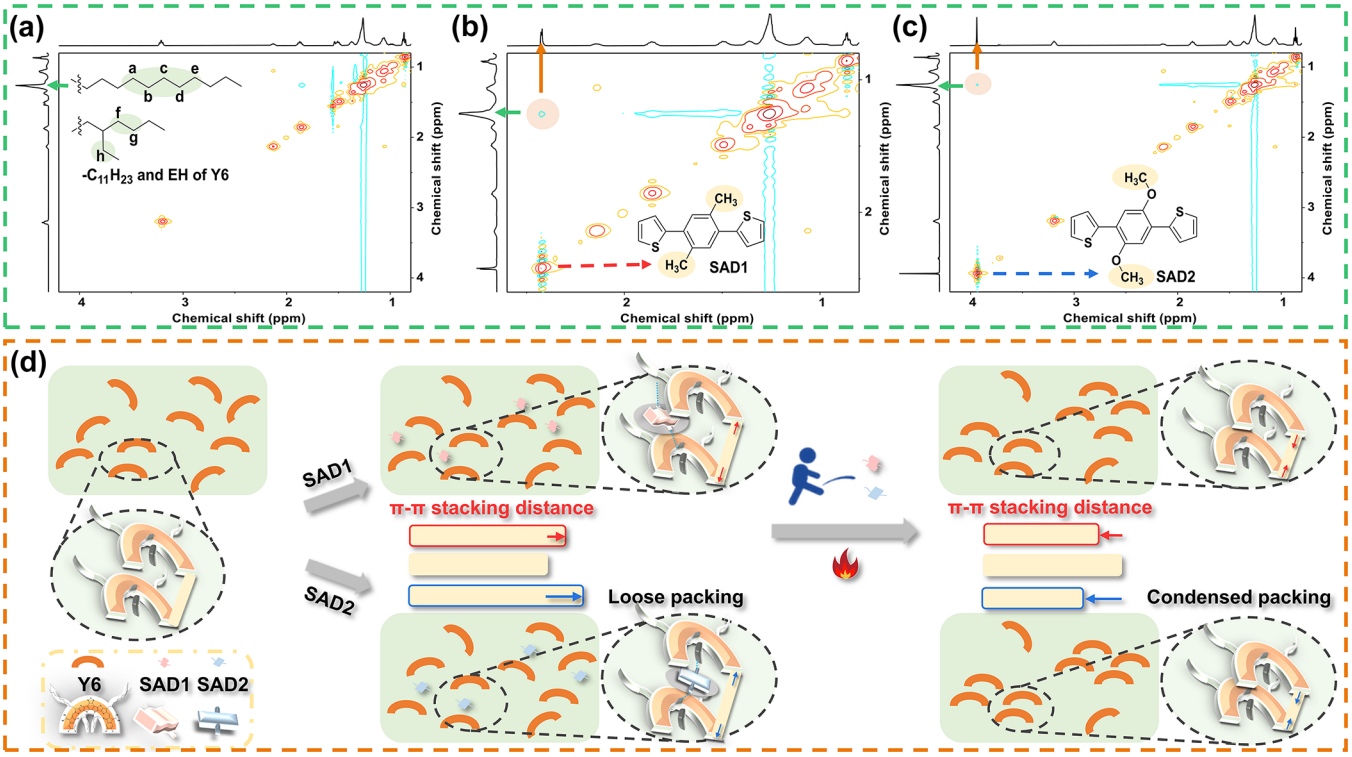

Figure 2. 2D ^{1}H−^{1}H NMR spectra of (a) Y6-0, (b) Y6-1, and (c) Y6-2 solutions. (d) Working mechanism diagram of the SAD treatment.

To investigate the volatilities of these two SADs, the TGA and UV−vis absorption were performed. As shown in Figure 1c, SAD1 and SAD2 were fully volatized when they were continuously heated to 220 and 270 °C, respectively, at a scan rate of 5 °C min^{-1}. Specifically, SAD1 and SAD2 could be volatilized completely when the temperature was held constant for 6 h at 100 and 140 °C, respectively. To further prove the complete removal of the SADs, the TGA of SAD-added PM6:Y6 blend films were measured. As shown in Figure S3, the TGA traces exhibited a ∼4% weight loss at 100 and 140 °C for SAD1- and SAD2-added PM6:Y6 films, which is well consistent with the content of the SADs, suggesting that the SADs could be completely removed from blend films. Due to the strong absorption in the UV region for both SADs, the absorption range from 300 to 400 nm is significantly enhanced in the PM6:Y6 blend films after the addition of SADs. Interestingly, the enhanced absorption gradually decreased until it fully disappeared when the SAD1-added (or SAD2-added) blend film was heated at 100 °C (or 140 °C) for 10 min, suggesting that the SADs were completely volatilized (Figure S4).

Conformation Effect of SADs on Y6. To explore the effects of conformations of SADs on Y6 film, the UV−vis absorption spectra of various films were carefully investigated (Figure 1d). To describe the process of adding and subsequently removing SADs for brevity and clarity, we named the various treatments as follows (by taking Y6 as an example). Y6-0, Y6-1, and Y6-2 refer to the as-cast Y6 film, SAD1-added Y6 film, and SAD2-added Y6 film, respectively. Y6-T0, Y6-T1, and Y6-T2 refer to the above Y6 films after the corresponding subsequent TA treatment (100 °C for 10 min, 100 °C for 10 min, 140 °C for 10 min, respectively). Similar to the reported results,[47] the absorption profile of the Y6-0 film consists of two main bands. One is the high-lying absorption band in the 300−420 nm region, which is attributed to the localized $\pi-\pi^*$ transition of the conjugated backbones. The other is the low-energy region of 420−920 nm with a λ_{max} value at 834 nm, ascribed to the intramolecular charge transfer between the central conjugated core and the end-groups. Compared with the λ_{max} value of the Y6-0 film, those values obviously blue-shifted by 12 nm for Y6-1 and 21 nm for Y6-2, implying that the original intermolecular packing of Y6 has been disturbed by the addition of SADs (Table S3).[48] The larger blue-shifted value of Y6-2 suggested SAD2 may disrupt the $\pi-\pi$ stacking of Y6 more severely. We thus argued that SAD2 may be able to insert between the Y6 molecules more efficiently due to its much more planar conformation. Furthermore, the absorption peak of Y6-T0 film exhibited a slight red-shift of 4 nm in comparison to that of Y6-0, indicating that the TA process has a negligible effect on the intermolecular packing of Y6. Impressively, after thermal removal of the SADs, the λ_{max} values largely red-shifted by 21 nm for Y6-T1 and by 28 nm for Y6-T2. In addition, the relative absorption intensity of 0−0 and 0−1 vibronic transition (I_{0-0}/I_{0-1}) increased from 1.58 (Y6-T0) to 1.62 (Y6-T1) and then to 1.68 (Y6-T2), suggesting the gradually improved molecular rigidity of Y6.[49] Based on absorption and emission spectra, the calculated $\Delta\nu$ values for and Y6-T2 (1308 cm^{-1}) were found to be much smaller than that for Y6-T0 (1462 cm^{-1}) and Y6-T1 (1336 cm^{-1}) (Figure S5). These results implied that the SAD2-treatment can reduce the reorganization energy and enhance the rigidity of Y6 more efficiently than SAD1-treatment.

Two-dimensional grazing-incidence wide-angle X-ray scattering (2D-GIWAXS) was conducted to further explore the influence of SAD conformations on the Y6 intermolecular packing modes (Figure S6 and Figure 1e). For Y6−0, a clear $\pi-\pi$ stacking (010) diffraction peak was observed at 1.74 Å^{-1}

https://doi.org/10.1021/jacs.2c05303
J. Am. Chem. Soc. 2022, 144, 14731−14739

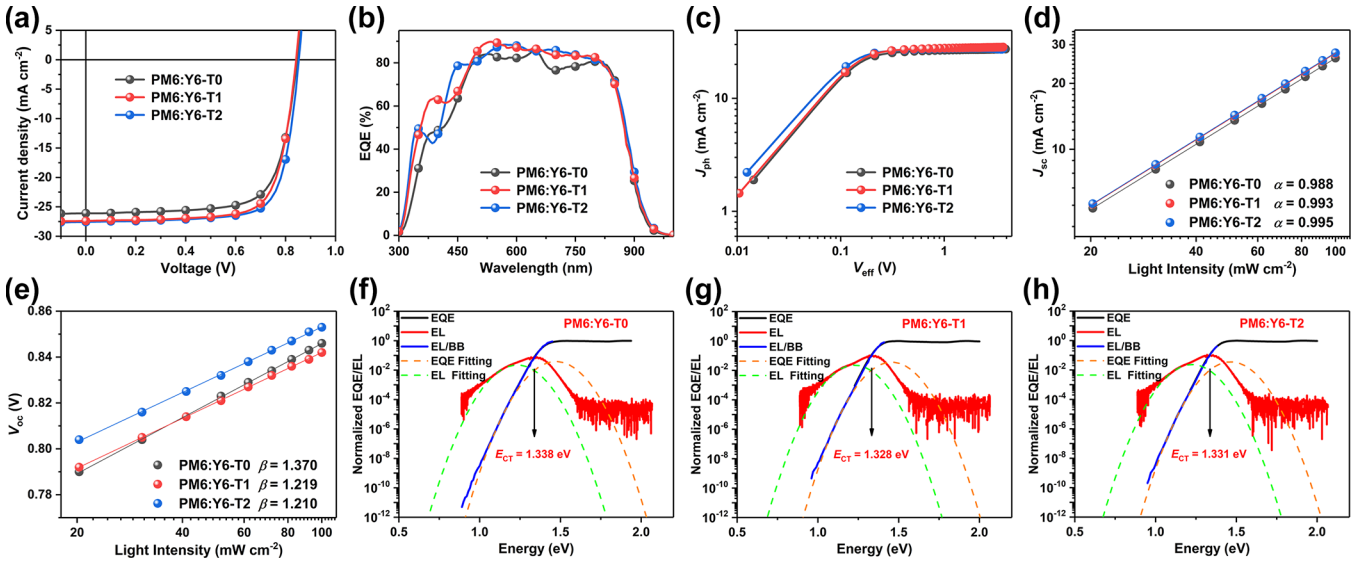

Figure 3. (a–e) J–V curves, EQE responses, photocurrent-effective voltage plots, light intensity-dependent J_{sc} curves, and light intensity-dependent V_{oc} curves of PM6:Y6-based devices processed with or w/o SADs. Normalized EL and EQE spectra of OSC devices based on (f) PM6:Y6-T0, (g) PM6:Y6-T1, and (h) PM6:Y6-T2.

Table 1. Photovoltaic Parameters of SAD-Treated OSCs Based on PM6:Y6 under AM1.5G Illumination, 100 mW cm^{-2}

active layers	V_{oc}[a] [V]	J_{sc}[a] [mA cm^{-2}]	calc J_{sc}[b] [mA cm^{-2}]	FF[a] [%]	PCE[a] [%]	V_{loss} [V]	ΔV_{nr} [V]
PM6:Y6-T0	0.846 (0.846 ± 0.001)	26.09 (26.02 ± 0.14)	25.18	72.62 (72.35 ± 0.65)	16.03 (15.93 ± 0.08)	0.540	0.212
PM6:Y6-T1	0.842 (0.842 ± 0.001)	27.38 (27.29 ± 0.17)	26.59	74.19 (74.13 ± 0.45)	17.10 (17.03 ± 0.05)	0.538	0.206
PM6:Y6-T2	0.853 (0.852 ± 0.001)	27.56 (27.49 ± 0.16)	26.69	75.46 (75.57 ± 0.49)	17.74 (17.69 ± 0.04)	0.532	0.198

[a]The average parameters were from 15 devices. [b]J_{sc} values calculated from EQE curves.

with a d-spacing of 3.61 Å in the out-of-plane (OOP) direction. After the addition of SADs, both films presented slightly larger d-spacing values (3.62 Å for Y6–1 and 3.63 Å for Y6–2, respectively), which is consistent with the blue-shifts of UV–vis absorption. After thermal-removal of SADs, both Y6-T1 and Y6-T2 films obviously exhibited a more condensed intermolecular packing mode than Y6-T0 (3.60 Å), which is beneficial to efficient charge transport. Specifically, the π–π stacking distance of Y6 in Y6-T2 (3.57 Å) is reduced to be slightly shorter than that in Y6-T1 (3.59 Å). These results suggested that the removal of SADs may enhance the π–π interactions in the Y6 film, while the removal of SAD2 is more efficient than SAD1.

To further understand the role of SADs, 2D ^{1}H–^{1}H NMR and Fourier-transform infrared spectroscopy (FTIR) analysis were performed to explore the intermolecular interaction between SADs and Y6.[50,51] Due to the nuclear Overhauser effect, the NOESY spectra can provide information about protons which are 5 Å or less apart in space.[52] Compared with the ^{1}H–^{1}H NMR spectra of pure Y6 in $CDCl_3$ solution (Figure 2a), an emerged cross-correlation resonance peak between CH_3– protons (2.42 ppm) of SAD1 and –CH_2– protons of Y6 (1.26 ppm, probably belonging to the protons from H_a to H_h) was clearly observed in the 2D ^{1}H–^{1}H NOESY spectra of Y6-1 solution (Figure 2b), while a similar NOE cross-peak between –OCH_3 protons (3.94 ppm) of SAD2 and –CH_2– protons of Y6 was also observed in Y6-2 solution (Figure 2c). In addition, FTIR results showed that the symmetrical stretching vibration (ν_s) of –CH_2– substituted on Y6 exhibited a red shift from 2855.1 cm^{-1} to 2854.6 and 2854.7 cm^{-1} after blending with SAD1 and SAD2, respectively (Figure S7). All these results confirm the existence of intermolecular interaction between Y6 and SADs in both solution and solid states.

Based on the above results, the working mechanism of the SAD treatment was proposed as shown in Figure 2d. In the solution, the pre-aggregates of Y6 are formed through H–H interactions with SADs. During the spin-coating process, the intermolecular interaction between Y6 and SAD1 (or SAD2) remains in the film state. Due to the planar conformation and relatively small space occupation, SAD2 can easily insert between Y6 molecules, while SAD1 with twisted conformation can only be interspersed around the Y6. Thus, the "π–π stacking distance" of Y6 molecules in Y6-T2 film became longer than that in Y6-T1 film. After TA treatment, both SAD1 and SAD2 are completely removed, resulting in a much tighter intermolecular packing mode of Y6. Specifically, the "π–π stacking distance" of Y6 molecules in Y6-T2 film became shorter than that in Y6-T1 film, beneficial to charge transport properties.

Effects of SAD Treatment on Photovoltaic Properties. To investigate the effect of the conformation of SADs on photovoltaic performance, the PM6:Y6 system was chosen to fabricate OSCs devices with a structure of ITO/PEDOT:PSS/PM6:Y6 (with or w/o the SAD treatment)/PDIN/Ag. The current density–voltage (J–V) curves and the summary of the detailed parameters are shown in Figure 3a, Table 1, and Tables S4 and S5. The optimal device based on PM6:Y6-T0 yielded a PCE of 16.03%, with an open-circuit voltage (V_{oc}) of 0.846 V, a short circuit current (J_{sc}) of 26.07 mA cm^{-2}, and a fill factor (FF) of 72.62%, similar to the previously reported values.[5,29] For the device based on PM6:Y6-T1, both the J_{sc}

https://doi.org/10.1021/jacs.2c05303
J. Am. Chem. Soc. 2022, 144, 14731–14739

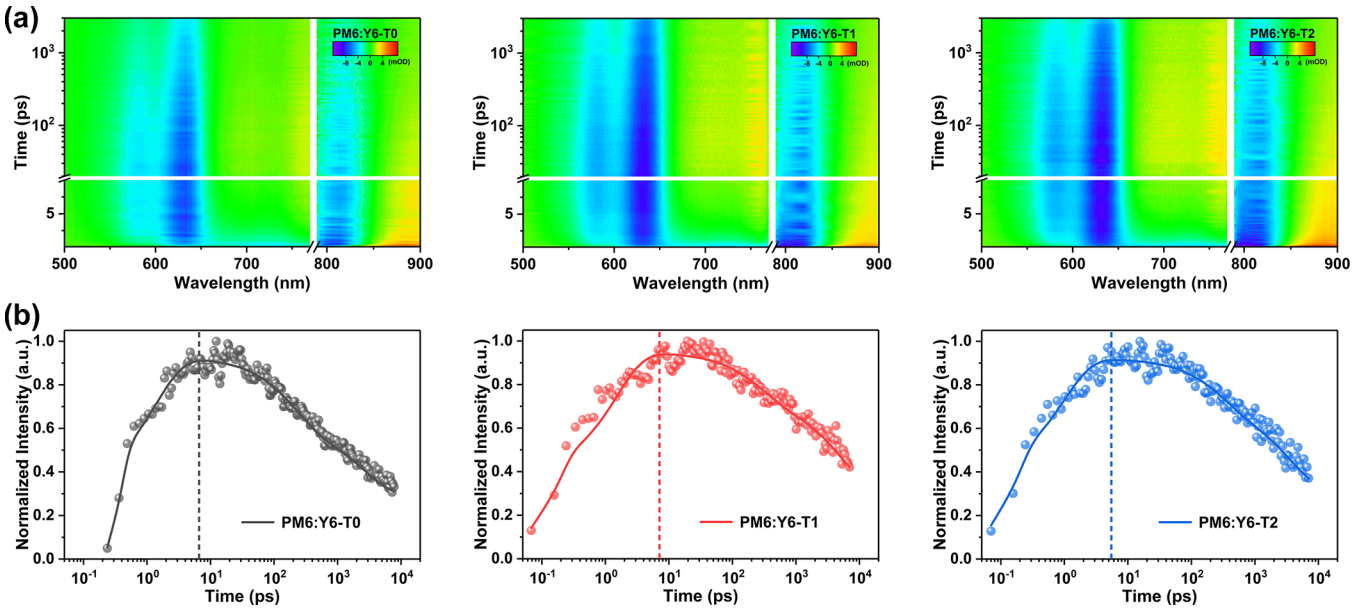

Figure 4. (a) 2D plots of TA spectra at an excitation wavelength of 800 nm. (b) TA kinetics of the hole transfer process for the corresponding blend films.

(27.38 mA cm^{-2}) and FF (74.19%) are simultaneously improved, thus leading to a good PCE of 17.10%, suggesting that SAD1 can boost the device efficiency. Furthermore, the PM6:Y6-T2-based device demonstrated a remarkable PCE of 17.74%, with further enhancement of V_{oc} (0.853 V) and FF (75.46%), which demonstrated that the planar SAD2 additive improved the device performance more efficiently than the twisted SAD1. Note that the 17.74% efficiency is the top result of PM6:Y6-based binary OSCs.[53,54] Figure 3b displays the external quantum efficiency (EQE) spectra of the three devices. The integrated J_{sc} values from the EQE response are calculated to be 25.18, 26.59, and 26.69 mA cm^{-2} for PM6:Y6-T0-, PM6:Y6-T1-, and PM6:Y6-T2-based OSCs, respectively, which are in accordance with the values obtained from the $J-V$ measurements within 5% mismatch.

To reveal the mechanism of the J_{sc} and FF in the devices, the charge generation and charge carrier transport and recombination were systematically studied. The charge separation properties of the three blend films were measured by the charge dissociation probability $P(E, T)$ as displayed in Figure 3c. Under short-circuit conditions, the $P(E, T)$ values are 96.6, 97.3, and 99.0% for PM6:Y6-T0, PM6:Y6-T1, and PM6:Y6-T2, respectively, which is consistent with the highest J_{sc} in PM6:Y6-T2-based devices. To investigate the charge transport properties, the hole and electron mobilities were measured by the space charge limited current method as shown in Figure S8. The hole mobilities of the three blends were similar, while the electron mobility increased from PM6:Y6-T0 (5.06×10^{-4} cm^2 V^{-1} s^{-1}) to PM6:Y6-T1 (5.21×10^{-4} cm^2 V^{-1} s^{-1}) and then to PM6:Y6-T2 (5.54×10^{-4} cm^2 V^{-1} s^{-1}), which is consistent with the order of $\pi-\pi$ stacking distances of Y6-T0, Y6-T1, and Y6-T2. The most balanced charge transport (μ_h/μ_e = 0.99) in the PM6:Y6-T2 blend films may contribute to the highest FF and J_{sc} among three OSCs. To further clarify the obvious changes in the J_{sc} and FF, the charge recombination was determined by measuring the J_{sc} and V_{oc} under various light intensities (P) from 100 to 20 mW cm^{-2}. The relationship between J_{sc} and P_{light} can be expressed as a power-law equation of $J_{sc} \propto P^{\alpha}$, which is used to analyze the bimolecular recombination in OSC devices (Figure 3d). The α values are determined to be 0.988, 0.993, and 0.995 for the PM6:Y6-T0-, PM6:Y6-T1-, and PM6:Y6-T2-based devices, respectively, implying that all the three devices present negligible bimolecular recombination. Furthermore, the recombination mechanism under open-circuit conditions can be described by the semi-logarithmic plots of the light-intensity-dependent V_{oc} experiments, giving the slope as $\beta kT/q$. Compared with that of the PM6:Y6-T0 device (1.370), the β values of PM6:Y6-T1 and PM6:Y6-T2 are 1.219 and 1.210, respectively, indicating the least trap-assisted Shockley–Read–Hall (SRH) recombination involved in SAD2-treated devices (Figure 3e). These results strongly support for the positive effects of SAD treatment on the improvement of J_{sc} and FF, while the SAD2 additive is more effective than SAD1.

To probe the mechanism of the differences in V_{oc}, the detailed voltage loss (V_{loss}) analysis of the three devices was performed. The total V_{loss} can be divided into three parts: the voltage loss due to charge generation ($\Delta E_{CT}/q$) and the radiative and nonradiative recombination voltage loss (ΔV_r and ΔV_{nr}). ΔE_{CT} stands for the difference between the energy of the bandgap of the blend film (E_g) and the energy of the charge transfer (CT) state (E_{CT}). The optical bandgap (E_g) of OSC devices were determined by the intersection of absorption and emission spectra of the Y6 film with or w/o the SAD treatment. As shown in Figure S9, the E_g values of Y6-T0, Y6-T1, and Y6-T2 are 1.386, 1.380, and 1.385 eV, respectively. Furthermore, the E_{CT} values of the three blend films were measured by employing the highly sensitive EQE and electroluminescence (EL) (Figure 3f–h). Accordingly, the E_{CT} values are 1.338, 1.328, and 1.331 eV for PM6:Y6-T0, PM6:Y6-T1, and PM6:Y6-T2, respectively, thus leading to near-zero $\Delta E_{CT}/q$ for all the three devices. In addition, there is negligible difference in the second part ΔV_r from the radiative recombination loss for the three devices (Table 1 and Table S6). Accordingly, the PM6:Y6-T2-based device possesses a smaller ΔV_{nr} (0.198 V) than PM6:Y6-T0 (0.212 V) and PM6:Y6-T1 (0.206 V), which is the main reason for the highest V_{oc} of 0.853 V.

https://doi.org/10.1021/jacs.2c05303
J. Am. Chem. Soc. 2022, 144, 14731–14739

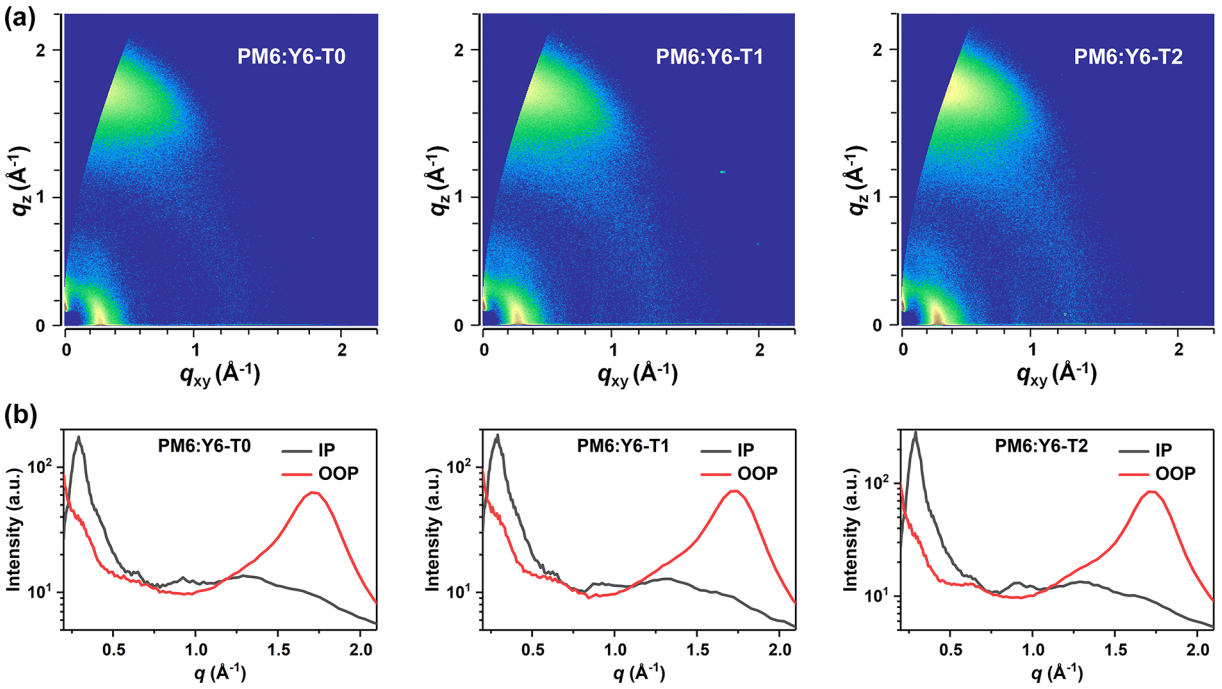

Figure 5. 2D-GIWAXS patterns (a) and the corresponding 1D line-cuts in the in-plane and out-of-plane directions (b) of PM6:Y6-T0, PM6:Y6-T1, and PM6:Y6-T2 blend films.

Table 2. Photovoltaic Parameters of Different SAD-Treated OSCs under AM1.5G Illumination, 100 mW cm^{-2}

active layers	V_{oc}[a] [V]	J_{sc}[a] [mA cm^{-2}]	calc J_{sc}[b] [mA cm^{-2}]	FF[a] [%]	PCE[a] [%]
PM6:BTP-eC9-T0	0.840 (0.840 ± 0.001)	25.72 (25.73 ± 0.16)	25.58	75.77 (75.30 ± 0.59)	16.37 (16.27 ± 0.09)
PM6: BTP-eC9-T1	0.838 (0.838 ± 0.001)	26.94 (26.84 ± 0.23)	25.74	77.45 (77.36 ± 0.50)	17.48 (17.40 ± 0.07)
PM6:BTP-eC9-T2	0.842 (0.842 ± 0.007)	27.22 (27.15 ± 0.13)	25.88	78.09 (77.78 ± 0.26)	17.90 (17.79 ± 0.08)
PM6:L8-BO-T0	0.883 (0.883 ± 0.001)	24.36 (24.38 ± 0.10)	23.98	77.39 (77.00 ± 0.38)	16.65 (16.57 ± 0.07)
PM6:L8-BO-T1	0.880 (0.880 ± 0.001)	26.40 (26.38 ± 0.10)	25.11	78.12 (77.82 ± 0.30)	18.15 (18.07 ± 0.08)
PM6:L8-BO-T2	0.889 (0.888 ± 0.001)	26.73 (26.68 ± 0.12)	25.43	79.32 (78.88 ± 0.50)	18.85 (18.68 ± 0.13)

[a]The average parameters were from 15 devices. [b]J_{sc} values calculated from EQE curves.

To understand the hole transfer (HT) dynamics of the three devices, femtosecond transient absorption (fs-TA) measurements were carried out on the blend films. The 2D plots of the blend films at 800 nm laser excitation to selectively excite the Y6 are shown in Figure 4a. The TA spectra exhibit negative signals at 770−850 nm, which match the ground state absorption spectra of Y6 well, thus being ascribable to the ground state bleaching (GSB) decay. In addition, new bleach signals in the region between 570 and 620 nm appear in the TA spectra of the three blends, which is consistent with the steady-state absorption features of PM6, suggesting an ultrafast HT process from Y6 to PM6. The HT dynamics in the blend films include not only the HT process from Y6 to PM6 but also the intrinsic relaxation of Y6.[55,56] The HT rate (k_{HT}) occurring at PM6:Y6 interfaces should be calculated by $k_{HT} = k_r - k_0$, where k_r is the total HT rate extracted from the PM6 decay process in the blend films and k_0 is the intrinsic HT rate extracted from the neat Y6 decay process. Thus, k_{HT} values of PM6:Y6-T0, PM6:Y6-T1, and PM6:Y6-T2 films are extracted at 600 nm with the gradually increased rates of 1.70×10^{12}, 2.85×10^{12}, and 3.47×10^{12} s^{-1}, respectively (Figure 4b and Table S7). Moreover, the estimated quantum efficiency (QE = k_{HT}/k_r) of photoinduced HT of PM6:Y6-T2 (96.7%) is relatively higher than those of PM6:Y6-T0 (91.4%) and PM6:Y6-T1 (95.3%). These findings revealed that PM6:Y6-T2 blend films possess the fastest and most effective HT process, which is well in line with the highest J_{sc}, most suppressed recombination loss, and highest PCE of the SAD2-treated OSC devices.

The influence of conformation of SAD on the blend film morphologies were investigated by 2D-GIWAXS (Figure 5a,b). A lamellar diffraction peak along the IP direction located at 0.29 Å was observed in all three blend films, which could be attributed to the overlap of the (100) stacking peak (PM6) and the (110) peak (Y6). Remarkably, obvious $\pi-\pi$ stacking (010) diffraction peaks were observed at q_z = 1.71 Å^{-1} (d = 3.67 Å, PM6:Y6-T0), 1.72 Å^{-1} (d = 3.65 Å, PM6:Y6-T1), and 1.73 Å^{-1} (d = 3.64 Å, PM6:Y6-T2). The corresponding crystallite coherence length (CCL_{010}) values, estimated from the Scherrer equation, are 25.31, 28.29, and 29.21 Å, respectively. This observation suggested that the planar SAD2 is beneficial to form a more ordered intermolecular packing mode than SAD1 in the PM6:Y6 blend films.

To explore the universal influence of the SAD conformation on photovoltaic performance, two derivatives of Y6 (BTP-eC9 and L8-BO) were also chosen as the acceptors for this study. The $J-V$ curves, EQE responses, and the corresponding device parameters of PM6:BTP-eC9 and PM6:L8-BO binary systems are shown in Figure S10 and Table 2. Obviously, all SAD-treated devices exhibited improved PCE with the increased J_{sc}

https://doi.org/10.1021/jacs.2c05303
J. Am. Chem. Soc. 2022, 144, 14731−14739

and FF. Moreover, the SAD2-treated devices showed better photovoltaic performance than those treated with SAD1. Impressively, PM6:L8-BO-T2-based devices presented an outstanding PCE of 18.85% (a certified value of 18.7% in the National Institute of Metrology, China; Figure S11), which is the record value for single-junction binary OSCs, revealing the superior performance of the planar-type SADs in enhancing photovoltaic performances.

CONCLUSIONS

In conclusion, two volatilizable SADs with different conformations were designed and synthesized to enhance the photovoltaic performance of OSCs. The conformation effect of SADs on the intermolecular packing modes of acceptors were systematically investigated theoretically and experimentally, which revealed that the planar SAD2 could more easily insert between Y6 molecules than SAD1, further inducing a tighter intermolecular packing mode of Y6 after the TA process, beneficial to the charge transport mobilities, thereby resulting in significantly enhanced PCE of OSCs. The universality of this mechanism was exemplified in several systems with a record efficiency (18.85%) of single-junction binary OSCs. The present work investigated the conformation effects of SADs on photovoltaic performances, which provides a new guideline to design SADs for high-performance OSCs.

ASSOCIATED CONTENT

Supporting Information

The Supporting Information is available free of charge at https://pubs.acs.org/doi/10.1021/jacs.2c05303.

Experimental details, device fabrication and characterization, and additional characterization, such as absorption spectra and emission spectra, FTIR, optical bandgaps, SCLC, GIWAXS, crystallographic data, certification report, ^{1}H and ^{13}C NMR spectra, and the optimization of the OSC devices (PDF)

Accession Codes

CCDC 2152137−2152138 contain the supplementary crystallographic data for this paper. These data can be obtained free of charge via www.ccdc.cam.ac.uk/data_request/cif, or by emailing data_request@ccdc.cam.ac.uk, or by contacting The Cambridge Crystallographic Data Centre, 12 Union Road, Cambridge CB2 1EZ, UK; fax: +44 1223 336033.

AUTHOR INFORMATION

Corresponding Authors

Xin Zhang − *College of Materials Science and Opto-Electronic Technology, Center of Materials Science and Optoelectronics Engineering, CAS Center for Excellence in Topological Quantum Computation, CAS Key Laboratory of Vacuum Physics, University of Chinese Academy of Sciences, Beijing 100190, China;* orcid.org/0000-0002-4611-0286; Email: zhangxin2019@ucas.ac.cn

Hui Huang − *College of Materials Science and Opto-Electronic Technology, Center of Materials Science and Optoelectronics Engineering, CAS Center for Excellence in Topological Quantum Computation, CAS Key Laboratory of Vacuum Physics, University of Chinese Academy of Sciences, Beijing 100190, China;* orcid.org/0000-0002-6102-2815; Email: huihuang@ucas.ac.cn

Authors

Congqi Li − *College of Materials Science and Opto-Electronic Technology, Center of Materials Science and Optoelectronics Engineering, CAS Center for Excellence in Topological Quantum Computation, CAS Key Laboratory of Vacuum Physics, University of Chinese Academy of Sciences, Beijing 100190, China*

Xiaobin Gu − *College of Materials Science and Opto-Electronic Technology, Center of Materials Science and Optoelectronics Engineering, CAS Center for Excellence in Topological Quantum Computation, CAS Key Laboratory of Vacuum Physics, University of Chinese Academy of Sciences, Beijing 100190, China*

Zhihao Chen − *School of Physics, State Key Laboratory of Crystal Materials, Shandong University, Jinan 250100 Shandong, China*

Xiao Han − *College of Materials Science and Opto-Electronic Technology, Center of Materials Science and Optoelectronics Engineering, CAS Center for Excellence in Topological Quantum Computation, CAS Key Laboratory of Vacuum Physics, University of Chinese Academy of Sciences, Beijing 100190, China*

Na Yu − *Center for Advanced Low-Dimension Materials, State Key Laboratory for Modification of Chemical Fibers and Polymer Materials, College of Materials Science and Engineering, Donghua University, Shanghai 201620, China*

Yanan Wei − *College of Materials Science and Opto-Electronic Technology, Center of Materials Science and Optoelectronics Engineering, CAS Center for Excellence in Topological Quantum Computation, CAS Key Laboratory of Vacuum Physics, University of Chinese Academy of Sciences, Beijing 100190, China*

Jinhua Gao − *College of Materials Science and Opto-Electronic Technology, Center of Materials Science and Optoelectronics Engineering, CAS Center for Excellence in Topological Quantum Computation, CAS Key Laboratory of Vacuum Physics, University of Chinese Academy of Sciences, Beijing 100190, China*

Hao Chen − *College of Materials Science and Opto-Electronic Technology, Center of Materials Science and Optoelectronics Engineering, CAS Center for Excellence in Topological Quantum Computation, CAS Key Laboratory of Vacuum Physics, University of Chinese Academy of Sciences, Beijing 100190, China*

Meng Zhang − *College of Materials Science and Opto-Electronic Technology, Center of Materials Science and Optoelectronics Engineering, CAS Center for Excellence in Topological Quantum Computation, CAS Key Laboratory of Vacuum Physics, University of Chinese Academy of Sciences, Beijing 100190, China*

Ao Wang − *College of Polymer Science and Engineering, State Key Laboratory of Polymer Materials Engineering, Sichuan University, Chengdu 610065, China*

Jianqi Zhang − *CAS Key Laboratory of Nanosystem and Hierarchical Fabrication, CAS Center for Excellence in Nanoscience, National Center for Nanoscience and Technology, Beijing 100190, China;* orcid.org/0000-0002-3549-1482

Zhixiang Wei − *CAS Key Laboratory of Nanosystem and Hierarchical Fabrication, CAS Center for Excellence in Nanoscience, National Center for Nanoscience and Technology, Beijing 100190, China;* orcid.org/0000-0001-6188-3634

https://doi.org/10.1021/jacs.2c05303
J. Am. Chem. Soc. 2022, 144, 14731−14739

Qian Peng − *School of Chemical Sciences, University of Chinese Academy of Sciences, Beijing 100190, China*
Zheng Tang − *Center for Advanced Low-Dimension Materials, State Key Laboratory for Modification of Chemical Fibers and Polymer Materials, College of Materials Science and Engineering, Donghua University, Shanghai 201620, China;* orcid.org/0000-0003-0036-2362
Xiaotao Hao − *School of Physics, State Key Laboratory of Crystal Materials, Shandong University, Jinan 250100 Shandong, China;* orcid.org/0000-0002-0197-6545

Complete contact information is available at: https://pubs.acs.org/10.1021/jacs.2c05303

Notes

The authors declare no competing financial interest.

■ ACKNOWLEDGMENTS

The authors acknowledge the financial support from the NSFC (52103352, 51925306, and 52120105006), National Key R&D Program of China (2018FYA 0305800), Key Research Program of Chinese Academy of Sciences (XDPB08-2), the Strategic Priority Research Program of Chinese Academy of Sciences (XDB28000000), the Youth Innovation Promotion Association of Chinese Academy of Sciences (2022165), and the Fundamental Research Funds for the Central Universities. DFT results described in this article were obtained from the National Supercomputing Center in Shenzhen (Shenzhen Cloud Computing Center).

■ REFERENCES

(1) Inganäs, O. Organic Photovoltaics over Three Decades. *Adv. Mater.* **2018**, *30*, 1800388.
(2) Liu, Y.; Liu, B.; Ma, C.; Huang, F.; Feng, G.; Chen, H.; Hou, J.; Yan, L.; Wei, Q.; Luo, Q.; Bao, Q.; Ma, W.; Liu, W.; Li, W.; Wan, X.; Hu, X.; Han, Y.; Li, Y.; Zhou, Y.; Zou, Y.; Chen, Y.; Li, Y.; Chen, Y.; Tang, Z.; Hu, Z.; Zhang, Z.; Bo, Z. Recent progress in organic solar cells (Part I material science). *Sci. China Chem.* **2022**, *65*, 224−268.
(3) Clarke, T. M.; Durrant, J. R. Charge Photogeneration in Organic Solar Cells. *Chem. Rev.* **2010**, *110*, 6736−6767.
(4) Yan, C.; Barlow, S.; Wang, Z.; Yan, H.; Jen, A. K. Y.; Marder, S. R.; Zhan, X. Non-fullerene acceptors for organic solar cells. *Nat. Rev. Mater.* **2018**, *3*, 18003.
(5) Yuan, J.; Zhang, Y.; Zhou, L.; Zhang, G.; Yip, H. L.; Lau, T. K.; Lu, X.; Zhu, C.; Peng, H.; Johnson, P. A.; Leclerc, M.; Cao, Y.; Ulanski, J.; Li, Y.; Zou, Y. Single-Junction Organic Solar Cell with over 15% Efficiency Using Fused-Ring Acceptor with Electron-Deficient Core. *Joule* **2019**, *3*, 1140−1151.
(6) Liu, Q.; Jiang, Y.; Jin, K.; Qin, J.; Xu, J.; Li, W.; Xiong, J.; Liu, J.; Xiao, Z.; Sun, K.; Yang, S.; Zhang, X.; Ding, L. 18% Efficiency organic solar cells. *Sci. Bull.* **2020**, *65*, 272−275.
(7) Li, C.; Zhou, J.; Song, J.; Xu, J.; Zhang, H.; Zhang, X.; Guo, J.; Zhu, L.; Wei, D.; Han, G.; Min, J.; Zhang, Y.; Xie, Z.; Yi, Y.; Yan, H.; Gao, F.; Liu, F.; Sun, Y. Non-fullerene acceptors with branched side chains and improved molecular packing to exceed 18% efficiency in organic solar cells. *Nat. Energy* **2021**, *6*, 605−613.
(8) Zheng, Z.; Wang, J.; Bi, P.; Ren, J.; Wang, Y.; Yang, Y.; Liu, X.; Zhang, S.; Hou, J. Tandem Organic Solar Cell with 20.2% Efficiency. *Joule* **2022**, *6*, 171−184.
(9) Wu, Z.; Sun, C.; Dong, S.; Jiang, X.; Wu, S.; Wu, H.; Yip, H. L.; Huang, F.; Cao, Y. n-Type Water/Alcohol-Soluble Naphthalene Diimide-Based Conjugated Polymers for High-Performance Polymer Solar Cells. *J. Am. Chem. Soc.* **2016**, *138*, 2004−2013.
(10) Zhang, Z.; Li, Y.; Cai, G.; Zhang, Y.; Lu, X.; Lin, Y. Selenium Heterocyclic Electron Acceptor with Small Urbach Energy for As-Cast High-Performance Organic Solar Cells. *J. Am. Chem. Soc.* **2020**, *142*, 18741−18745.
(11) Sariciftci, N. S.; Smilowitz, L.; Heeger, A. J.; Wudl, F. Photoinduced Electron Transfer from a Conducting Polymer to Buckminsterfullerene. *Science* **1992**, *258*, 1474−1476.
(12) Zhu, L.; Zhang, M.; Zhong, W.; Leng, S.; Zhou, G.; Zou, Y.; Su, X.; Ding, H.; Gu, P.; Liu, F.; Zhang, Y. Progress and prospects of the morphology of non-fullerene acceptor based high-efficiency organic solar cells. *Energy Environ. Sci.* **2021**, *14*, 4341−4357.
(13) Wei, Y.; Yu, J.; Qin, L.; Chen, H.; Wu, X.; Wei, Z.; Zhang, X.; Xiao, Z.; Ding, L.; Gao, F.; Huang, H. A universal method for constructing high efficiency organic solar cells with stacked structures. *Energy Environ. Sci.* **2021**, *14*, 2314−2321.
(14) Gao, J.; Gao, W.; Ma, X.; Hu, Z.; Xu, C.; Wang, X.; An, Q.; Yang, C.; Zhang, X.; Zhang, F. Over 14.5% efficiency and 71.6% fill factor of ternary organic solar cells with 300 nm thick active layers. *Energy Environ. Sci.* **2020**, *13*, 958−967.
(15) Zhu, W.; Spencer, A. P.; Mukherjee, S.; Alzola, J. M.; Sangwan, V. K.; Amsterdam, S. H.; Swick, S. M.; Jones, L. O.; Heiber, M. C.; Herzing, A. A.; Li, G.; Stern, C. L.; DeLongchamp, D. M.; Kohlstedt, K. L.; Hersam, M. C.; Schatz, G. C.; Wasielewski, M. R.; Chen, L. X.; Facchetti, A.; Marks, T. J. Crystallography, Morphology, Electronic Structure, and Transport in Non-Fullerene/Non-Indacenodithieno-thiophene Polymer:Y6 Solar Cells. *J. Am. Chem. Soc.* **2020**, *142*, 14532−14547.
(16) Liao, H. C.; Ho, C. C.; Chang, C. Y.; Jao, M. H.; Darling, S. B.; Su, W. Additives for morphology control in high-efficiency organic solar cells. *Mater. Today* **2013**, *16*, 326−336.
(17) Peet, J.; Kim, J. Y.; Coates, N. E.; Ma, W. L.; Moses, D.; Heeger, A. J.; Bazan, G. C. Efficiency enhancement in low-bandgap polymer solar cells by processing with alkane dithiols. *Nat. Mater.* **2007**, *6*, 497−500.
(18) Lee, J. K.; Ma, W. L.; Brabec, C. J.; Yuen, J.; Moon, J. S.; Kim, J. Y.; Lee, K.; Bazan, G. C.; Heeger, A. J. Processing Additives for Improved Efficiency from Bulk Heterojunction Solar Cells. *J. Am. Chem. Soc.* **2008**, *130*, 3619−3623.
(19) Ma, W.; Yang, C.; Gong, X.; Lee, K.; Heeger, A. J. Thermally Stable, Efficient Polymer Solar Cells with Nanoscale Control of the Interpenetrating Network Morphology. *Adv. Funct. Mater.* **2005**, *15*, 1617−1622.
(20) Li, M.; Liu, F.; Wan, X.; Ni, W.; Kan, B.; Feng, H.; Zhang, Q.; Yang, X.; Wang, Y.; Zhang, Y.; Shen, Y.; Russell, T. P.; Chen, Y. Subtle Balance Between Length Scale of Phase Separation and Domain Purification in Small-Molecule Bulk-Heterojunction Blends under Solvent Vapor Treatment. *Adv. Mater.* **2015**, *27*, 6296−6302.
(21) Yu, R.; Yao, H.; Hong, L.; Qin, Y.; Zhu, J.; Cui, Y.; Li, S.; Hou, J. Design and application of volatilizable solid additives in non-fullerene organic solar cells. *Nat. Commun.* **2018**, *9*, 4645.
(22) Liu, L.; Kan, Y.; Gao, K.; Wang, J.; Zhao, M.; Chen, H.; Zhao, C.; Jiu, T.; Jen, A. K. Y.; Li, Y. Graphdiyne Derivative as Multifunctional Solid Additive in Binary Organic Solar Cells with 17.3% Efficiency and High Reproductivity. *Adv. Mater.* **2020**, *32*, 1907604.
(23) Guo, Q.; Liu, Y.; Liu, M.; Zhang, H.; Qian, X.; Yang, J.; Wang, J.; Xue, W.; Zhao, Q.; Xu, X.; Ma, W.; Tang, Z.; Li, Y.; Bo, Z. Enhancing the Performance of Organic Solar Cells by Prolonging the Lifetime of Photogenerated Excitons. *Adv. Mater.* **2020**, *32*, 2003164.
(24) Fu, J.; Chen, S.; Yang, K.; Jung, S.; Lv, J.; Lan, L.; Chen, H.; Hu, D.; Yang, Q.; Duan, T.; Kan, Z.; Yang, C.; Sun, K.; Lu, S.; Xiao, Z.; Li, Y. A "σ-Hole"-Containing Volatile Solid Additive Enabling 16.5% Efficiency Organic Solar Cells. *iScience* **2020**, *23*, 100965.
(25) Yu, R.; Yao, H.; Xu, Y.; Li, J.; Hong, L.; Zhang, T.; Cui, Y.; Peng, Z.; Gao, M.; Ye, L.; Tan, Z. a.; Hou, J. Quadrupole Moment Induced Morphology Control Via a Highly Volatile Small Molecule in Efficient Organic Solar Cells. *Adv. Funct. Mater.* **2021**, *31*, 2010535.
(26) Fu, J.; Chen, H.; Huang, P.; Yu, Q.; Tang, H.; Chen, S.; Jung, S.; Sun, K.; Yang, C.; Lu, S.; Kan, Z.; Xiao, Z.; Li, G. Eutectic phase behavior induced by a simple additive contributes to efficient organic solar cells. *Nano Energy* **2021**, *84*, 105862.

(27) Cai, J.; Wang, H.; Zhang, X.; Li, W.; Li, D.; Mao, Y.; Du, B.; Chen, M.; Zhuang, Y.; Liu, D.; Qin, H.-L.; Zhao, Y.; Smith, J. A.; Kilbride, R. C.; Parnell, A. J.; Jones, R. A. L.; Lidzey, D. G.; Wang, T. Fluorinated solid additives enable high efficiency non-fullerene organic solar cells. *J. Mater. Chem. A* **2020**, *8*, 4230−4238.
(28) Zhang, X.; Cai, J.; Guo, C.; Li, D.; Du, B.; Zhuang, Y.; Cheng, S.; Wang, L.; Liu, D.; Wang, T. Simultaneously Enhanced Efficiency and Operational Stability of Nonfullerene Organic Solar Cells via Solid-Additive-Mediated Aggregation Control. *Small* **2021**, *17*, 2102558.
(29) Fan, H.; Yang, H.; Wu, Y.; Yildiz, O.; Zhu, X.; Marszalek, T.; Blom, P. W. M.; Cui, C.; Li, Y. Anthracene-Assisted Morphology Optimization in Photoactive Layer for High-Efficiency Polymer Solar Cells. *Adv. Funct. Mater.* **2021**, *31*, 2103944.
(30) Bao, S.; Yang, H.; Fan, H.; Zhang, J.; Wei, Z.; Cui, C.; Li, Y. Volatilizable Solid Additive-Assisted Treatment Enables Organic Solar Cells with Efficiency over 18.8% and Fill Factor Exceeding 80%. *Adv. Mater.* **2021**, *33*, 2105301.
(31) Huang, H.; Guo, Q.; Feng, S.; Zhang, C.; Bi, Z.; Xue, W.; Yang, J.; Song, J.; Li, C.; Xu, X.; Tang, Z.; Ma, W.; Bo, Z. Noncovalently fused-ring electron acceptors with near-infrared absorption for high-performance organic solar cells. *Nat. Commun.* **2019**, *10*, 3038.
(32) Yu, Z.; Liu, Z.; Chen, F.; Qin, R.; Lau, T. K.; Yin, J.; Kong, X.; Lu, X.; Shi, M.; Li, C.; Chen, H. Simple non-fused electron acceptors for efficient and stable organic solar cells. *Nat. Commun.* **2019**, *10*, 2152.
(33) Zhang, X.; Qin, L.; Yu, J.; Li, Y.; Wei, Y.; Liu, X.; Lu, X.; Gao, F.; Huang, H. High-Performance Noncovalently Fused-Ring Electron Acceptors for Organic Solar Cells Enabled by Noncovalent Intramolecular Interactions and End-Group Engineering. *Angew. Chem., Int. Ed.* **2021**, *60*, 12475−12481.
(34) Dong, T.; Lv, L.; Feng, L.; Xia, Y.; Deng, W.; Ye, P.; Yang, B.; Ding, S.; Facchetti, A.; Dong, H.; Huang, H. Noncovalent Se···O Conformational Locks for Constructing High-Performing Optoelectronic Conjugated Polymers. *Adv. Mater.* **2017**, *29*, 1606025.
(35) Vegiraju, S.; Chang, B. C.; Priyanka, P.; Huang, D.; Wu, K.; Li, L.; Chang, W. C.; Lai, Y. Y.; Hong, S.; Yu, B. C.; Wang, C. L.; Chang, W. J.; Liu, C.; Chen, M.; Facchetti, A. Intramolecular Locked Dithioalkylbithiophene-Based Semiconductors for High-Performance Organic Field-Effect Transistors. *Adv. Mater.* **2017**, *29*, 1702414.
(36) Yang, J.; Zhao, Z.; Geng, H.; Cheng, C.; Chen, J.; Sun, Y.; Shi, L.; Yi, Y.; Shuai, Z.; Guo, Y.; Wang, S.; Liu, Y. Isoindigo-Based Polymers with Small Effective Masses for High-Mobility Ambipolar Field-Effect Transistors. *Adv. Mater.* **2017**, *29*, 1702115.
(37) Lei, T.; Dou, J.-H.; Ma, Z.-J.; Yao, C.-H.; Liu, C.-J.; Wang, J.-Y.; Pei, J. Ambipolar Polymer Field-Effect Transistors Based on Fluorinated Isoindigo: High Performance and Improved Ambient Stability. *J. Am. Chem. Soc.* **2012**, *134*, 20025−20028.
(38) Jiang, G.; Li, Q.; Lv, A.; Liu, L.; Gong, J.; Ma, H.; Wang, J.; Tang, B. Z. Modulation of the intramolecular hydrogen bonding and push−pull electron effects toward realizing highly efficient organic room temperature phosphorescence. *J. Mater. Chem. C* **2022**, DOI: 10.1039/D2TC01093C.
(39) Liu, Z.; Hu, J.; Huang, C.; Huang, T. H.; Chen, D.; Ho, S. Y.; Chen, K. Y.; Li, E. Y.; Chou, P.-T. Sulfur-Based Intramolecular Hydrogen-Bond: Excited-State Hydrogen-Bond On/Off Switch with Dual Room-Temperature Phosphorescence. *J. Am. Chem. Soc.* **2019**, *141*, 9885−9894.
(40) Lv, L.; Yu, J.; Sui, X.; Wu, J.; Dong, X.; Lu, G.; Liu, X.; Peng, A.; Huang, H. Significant enhancement of responsivity of organic photodetectors upon molecular engineering. *J. Mater. Chem. C* **2019**, *7*, 5739−5747.
(41) Huang, H.; Chen, Z.; Ortiz, R. P.; Newman, C.; Usta, H.; Lou, S.; Youn, J.; Noh, Y. Y.; Baeg, K. J.; Chen, L. X.; Facchetti, A.; Marks, T. J. Combining Electron-Neutral Building Blocks with Intramolecular "Conformational Locks" Affords Stable, High-Mobility P- and N-Channel Polymer Semiconductors. *J. Am. Chem. Soc.* **2012**, *134*, 10966−10973.
(42) Yu, S.; Peng, A.; Zhang, S.; Huang, H. Noncovalent conformational locks in organic semiconductors. *Sci. China Chem.* **2018**, *61*, 1359−1367.
(43) Huang, H.; Yang, L.; Facchetti, A.; Marks, T. J. Organic and Polymeric Semiconductors Enhanced by Noncovalent Conformational Locks. *Chem. Rev.* **2017**, *117*, 10291−10318.
(44) Zhang, X.; Li, C.; Qin, L.; Chen, H.; Yu, J.; Wei, Y.; Liu, X.; Zhang, J.; Wei, Z.; Gao, F.; Peng, Q.; Huang, H. Side-Chain Engineering for Enhancing the Molecular Rigidity and Photovoltaic Performance of Noncovalently Fused-Ring Electron Acceptors. *Angew. Chem., Int. Ed.* **2021**, *60*, 17720−17725.
(45) Yang, L.; Ye, P.; Li, W.; Zhang, W.; Guan, Q.; Ye, C.; Dong, T.; Wu, X.; Zhao, W.; Gu, X.; Peng, Q.; Tang, B.; Huang, H. Uncommon Aggregation-Induced Emission Molecular Materials with Highly Planar Conformations. *Adv. Opt. Mater.* **2018**, *6*, 1701394.
(46) Lois, S.; Florès, J.-C.; Lère-Porte, J.-P.; Serein-Spirau, F.; Moreau, J. J. E.; Miqueu, K.; Sotiropoulos, J.-M.; Baylère, P.; Tillard, M.; Belin, C. How to Build Fully π-Conjugated Architectures with Thienylene and Phenylene Fragments. *Eur. J. Org. Chem.* **2007**, *2007*, 4019−4031.
(47) Liu, W.; Liu, Q.; Xiang, C.; Zhou, H.; Jiang, L.; Zou, Y. Theoretical exploration of optoelectronic performance of PM6:Y6 series-based organic solar cells. *Surf. Interfaces* **2021**, *26*, 101385.
(48) Kadem, B.; Hassan, A.; Cranton, W. Efficient P3HT:PCBM bulk heterojunction organic solar cells; effect of post deposition thermal treatment. *J. Mater. Sci.: Mater. Electron.* **2016**, *27*, 7038−7048.
(49) Spano, F. C.; Silva, C. H- and J-Aggregate Behavior in Polymeric Semiconductors. *Annu. Rev. Phys. Chem.* **2014**, *65*, 477−500.
(50) Chen, H.; Zhang, R.; Chen, X.; Zeng, G.; Kobera, L.; Abbrent, S.; Zhang, B.; Chen, W.; Xu, G.; Oh, J.; Kang, S. H.; Chen, S.; Yang, C.; Brus, J.; Hou, J.; Gao, F.; Li, Y.; Li, Y. A guest-assisted molecular-organization approach for >17% efficiency organic solar cells using environmentally friendly solvents. *Nat. Energy* **2021**, *6*, 1045−1053.
(51) Du, X.; Lu, X.; Zhao, J.; Zhang, Y.; Li, X.; Lin, H.; Zheng, C.; Tao, S. Hydrogen Bond Induced Green Solvent Processed High Performance Ternary Organic Solar Cells with Good Tolerance on Film Thickness and Blend Ratios. *Adv. Funct. Mater.* **2019**, *29*, 1902078.
(52) Oschkinat, H.; Griesinger, C.; Kraulis, P. J.; Sørensen, O. W.; Ernst, R. R.; Gronenborn, A. M.; Clore, G. M. Three-dimensional NMR spectroscopy of a protein in solution. *Nature* **1988**, *332*, 374−376.
(53) Huang, J.; Zhao, D.; Dou, Z.; Fan, Q.; Li, N.; Peng, S.; Liu, H.; Jiang, Y.; Yu, J.; Li, C. Highly efficient ITO-free organic solar cells with a column-patterned microcavity. *Energy Environ. Sci.* **2021**, *14*, 3010−3018.
(54) Lv, J.; Tang, H.; Huang, J.; Yan, C.; Liu, K.; Yang, Q.; Hu, D.; Singh, R.; Lee, J.; Lu, S.; Li, G.; Kan, Z. Additive-induced miscibility regulation and hierarchical morphology enable 17.5% binary organic solar cells. *Energy Environ. Sci.* **2021**, *14*, 3044−3052.
(55) Zhou, G.; Zhang, M.; Chen, Z.; Zhang, J.; Zhan, L.; Li, S.; Zhu, L.; Wang, Z.; Zhu, X.; Chen, H.; Wang, L.; Liu, F.; Zhu, H. Marcus Hole Transfer Governs Charge Generation and Device Operation in Nonfullerene Organic Solar Cells. *ACS Energy Lett.* **2021**, *6*, 2971−2981.
(56) Niu, M.; Wang, K.; Yang, X.; Bi, P.; Zhang, K.; Feng, X.; Chen, F.; Qin, W.; Xia, J.; Hao, X. Correction to "Hole Transfer Originating from Weakly Bound Exciton Dissociation in Acceptor−Donor−Acceptor Nonfullerene Organic Solar Cells.". *J. Phys. Chem. Lett.* **2020**, *11*, 831−831.